Developments in the Built Environment 18 (2024) 100416

Contents lists available at ScienceDirect

Developments in the Built Environment

journal homepage: www.sciencedirect.com/journal/developments-in-the-built-environment

Investigation on NTC/PTC effects of cement-based self-heating composites with varied conductive filler contents

H.N. Yoon [a], Jinho Bang [b], Daeik Jang [c,**], Beomjoo Yang [b,*]

[a] Construction Material Center, Construction Safety Research Institute Korea Testing & Research Institute 68, Gajaeul-ro, Seo-gu, Inchenon, 22829, Republic of Korea
[b] School of Civil Engineering, Chungbuk National University 1 Chungdae-ro, Seowon-gu, Cheongju, Chungbuk, 28644, Republic of Korea
[c] Department of Civil and Environmental Engineering, University of Pittsburgh, Pittsburgh, PA, 15261, USA

ARTICLE INFO

Keywords:
Cementitious composite
Carbon nanotube
Carbon fiber
Electric heating
Electrical resistivity

ABSTRACT

The present study systematically investigated the influence of varied conductive filler contents on the negative/positive temperature coefficient (NTC/PTC) effects in cement-based self-heating composites. Different composite formulations containing varying proportions of carbon nanotubes (CNT) and carbon fiber (CF) were prepared and subjected to self-heating tests at different input voltages. Analysis of temperature and electrical conductivity data obtained during the tests elucidated the NTC/PTC effects. Additionally, diverse analytical techniques were employed to characterize the physicochemical properties of the samples. Results indicated a correlation between NTC and PTC effects and thermal expansion as well as variations in electrical resistivity with increasing temperature. Moreover, a specific temperature and electrical resistivity range is identified where the NTC effect transitions to the PTC effect, a transition range influenced by the conductive filler content. Enhanced heat-generation accelerated the PTC effect by inducing structural alterations in the sample's physicochemical composition.

1. Introduction

Current research efforts extensively utilize carbon nanotubes (CNT) in the fabrication of functional composites with self-heating capabilities, leveraging their outstanding electrical, mechanical, and thermal properties (Chu and Park, 2016; Chien et al., 2014; Ding et al., 2022). Early studies focused on CNT-incorporated composites based on polymer matrices; however, recent studies have shifted their focus towards the development of CNT-incorporated composites based on cement matrices for applications as heating materials (Kim et al., 2016; Lee et al., 2020a; Jang et al., 2021a). Numerous investigations on CNT-incorporated cementitious composites for electric heating found that the heat generation of composites improved with increasing CNT content, and the uniform dispersion of CNT in the cement matrix, as well as the excellent conductivity of the composites, were identified as crucial factors for enhancing the heating performance (Jeong and Jeon, 2013; Meng et al., 2017; Jang et al., 2023a).

Research has been conducted to explore the enhancement of electrical conductivity in composites through the addition of carbon fiber (CF) (Zhou et al., 2016; Azhari and Banthia, 2012; Shin et al., 2015). It has been reported that the addition of CF to cementitious composites with CNT significantly improves both the electrical conductivity and stability, owing to the synergistic effect of micro-sized CF and nano-sized CNT (Zhou et al., 2016; Azhari and Banthia, 2012; Shin et al., 2015). For instance, Ding et al. and Kim et al. have reported that introducing CF into CNT/cement composites results in the creation of hierarchical conductive networks, enhancing not only electrical conductivity but also functional attributes such as self-sensing ability and heat-generation performance. (Ding et al., 2023; Kim et al., 2017). In addition, the formation of expanded electrically conductive networks by micro-sized CF counteracts the decrease in electrical conductivity caused by the evaporation of the electrolytic pore solution (Kim et al., 2017). A study on the heat generation of cementitious composites with CNT and CF demonstrated that the addition of CF enhances both the heat generation capability and stability of the composite (Kim et al., 2018). This enhancement is attributed to the reduced damage to the electrically conductive pathways through the formation of overlapping conductive pathways consisting of CNT and CF (Kim et al., 2018).

The effects of negative temperature coefficient (NTC) and positive temperature coefficient (PTC) on the heating stability of composites

* Corresponding author.
** Corresponding author.
E-mail addresses: daeik.jang@pitt.edu (D. Jang), byang@cbnu.ac.kr (B. Yang).

https://doi.org/10.1016/j.dibe.2024.100416
Received 4 January 2024; Received in revised form 11 March 2024; Accepted 22 March 2024
Available online 26 March 2024

Table 1
Mix proportions of CNT- and CF-incorporated cementitious composites.

Group	Sample ID	Cement	Silica fume	CNT	CF	Water	SP
A	N0F0	100	10	0	0	30	0
	N1F0			0.1			0.3
	N2F0			0.2			0.5
	N3F0			0.3			0.8
	N4F0			0.4			1.0
	N5F0			0.5			1.3
	N6F0			0.6			1.6
	N10F0			1.0			2.5
B	N6F0	100	10	0.6	0	30	1.6
	N5F1			0.5	0.1		1.3
	N4F2			0.4	0.2		1.0
	N3F3			0.3	0.3		0.8
	N2F4			0.2	0.4		0.5
	N1F5			0.1	0.5		0.3
	N0F6			0	0.6		0
C	N0F0	100	10	0	0	30	0
	N0F1				0.1		
	N0F3				0.3		
	N0F6				0.5		
	N0F10				0		
D	N6F0	100	10	0.6	0	30	1.6
	N6F1				0.3		
	N6F3				0.6		
	N6F5				1.0		

have garnered steady interest in the field of electric heating composites (Xiang et al., 2009; Kil et al., 2022). The NTC effect refers to the decrease in electrical resistance with increasing temperature, while the PTC effect corresponds to an increase in resistance (Kil et al., 2022; Jang et al., 2022a). Several studies in the field of polymeric composites have revealed that composites containing conductive fillers can exhibit various NTC or PTC effects, which are dependent on the properties of the polymer, including the coefficient of thermal expansion, melting point, and glass transition temperature, as well as the shape of the conductive filler (Neitzert et al., 2011). Therefore, in order to enhance the heating performance and stability of electric heating composites, a comprehensive understanding of the effects of NTC and PTC is crucial.

Until recently, studies on cementitious composites incorporating CNT have primarily focused on achieving a uniform dispersion of CNT within the cement matrix and assessing the heating performance of the composites. However, limited attention has been given to investigating the changes in electrical resistance and physicochemical structure induced by electric heating. Specifically, the effects of NTC and PTC, which are crucial for ensuring the heating stability of CNT-incorporated cementitious composites, have not been extensively explored. In addition, while the NTC/PTC effects are associated with changes in the matrix of cementitious composites induced by heating, there is still a lack of research on the physicochemical changes occurring in the cement matrix due to electric heating (Liu et al., 2019).

In this regard, the present study investigates the influence of conductive filler content on NTC/PTC effects and microstructural changes in conductive cement composites under electric heating conditions. Composites containing various amounts of CNT and CF were fabricated, and a monotonic heating test was conducted at different input voltages. The electric heating performance and NTC/PTC effect of the composites were analyzed using the temperature and electrical resistance data collected during the heating test. The physicochemical structure of the composites before and after the heating test was characterized using X-ray diffraction (XRD), thermogravimetric analysis (TG), and mercury intrusion porosimetry (MIP).

2. Experimental procedure

2.1. Materials and sample preparation

Ordinary Portland cement was used as a binder material. Electrical conductive fillers, multi-walled CNT and polyacrylonitrile (PAN)-based CF (fabricated form JEIO Co., Ltd. (JENOTUBE 8A) and Ace C&TECH. Co., Ltd. (ACECA), respectively) were used in this study (Yoon et al., 2021). The CNT had a length of 100-200 μm and a diameter of 6-9 nm, while the CF had a length of 3 mm and a diameter of 6-7 μm. Silica fume (Elkem Inc., EMS-940U) with a particle size ranging from 5 to 10 μm and polycarboxylate-based superplasticizer (SP) were used as dispersion agents (Jang et al., 2021b, 2024). The mix proportions of the CNT- and CF-incorporated cementitious composites are listed in Table 1. The composites were divided into four groups based on the mix proportions. Group A consisted of composites with mix proportions containing 0–1.0 wt% of CNT, while group B had a fixed mix proportion with a content of 0.6 wt% of the conductive filler, where CNT were replaced by CF. Group C had a mix proportion containing 0–1.0 wt% of CF, and finally, in the mix proportion of group D, the content of CNT was fixed at 0.6 wt%, and CF were added incrementally from 0 to 0.5 wt%. The silica fume content and water-to-cement ratio were maintained at 10.0 wt% and 0.3, respectively. The amount of SP was adjusted in proportion to the CNT content, either increased or decreased.

The mixing method of the samples was as follows: Dry materials (i.e., cement, silica fume, conductive fillers) were placed into a Hobart mixer and dry mixing was conducted for 5 min. Subsequently, water and SP were added and mixed for 5 min. The samples were cast in 50 × 50 × 50 mm^3 molds. Two copper electrodes with a size of 30 × 70 mm^2 were positioned in the middle of the specimen, maintaining a 20 mm spacing between them. After 24 h, the samples were demolded and sealed with plastic wrap and cured in an oven at 25 ± 3 °C for 28 days (Yoon et al., 2023).

2.2. Test methods

After 28 days of curing, the electrical resistance was measured utilizing a handheld digital multimeter (Keysight U1282A) and was converted to electrical resistivity. Details of the equation used to convert resistance to the resistivity can be found in Jang et al., 2023b, 2023c. Afterward, the cured specimens were subjected to a drying process in an oven maintained at a temperature of 60 ± 3 °C for a duration of three days (Yoon et al., 2023). This step was implemented to prevent any alterations in electrical conductivity that could arise from residual moisture present in the samples. The electrical resistance of the samples that underwent drying in the oven was subsequently measured. Three samples were measured for each mix proportion, and the average value was calculated.

For the monotonic heating test, the samples were subjected to an input voltage of 3–8 V for 1 h using a DC power supply. A K-type thermocouple was affixed to the surface of the samples to measure the temperature of the samples. A data logger (Agilent Technologies 34972A) linked to the DC power supply and thermocouples recorded the electrical current and temperature of the samples. The heating test was performed on three samples for each mix proportion, and the average value was calculated. The ambient temperature during the heating test was 25 ± 3 °C. In this study, identical experimental setups were employed, consistent with the protocols outlined in previous studies conducted by the authors. (Jang et al., 2022a, 2023d).

XRD, TG, and MIP analyses were conducted on selected samples to examine the changes in the physicochemical structure before and after the heating test. Fractures between the electrodes in the samples before and after the heating test were collected, and subjected preconditioning. The fractured samples were ground to a particle size of less than 64 μm for the XRD and TG analyses, and the powder samples were immersed in isopropanol for the solvent exchange method. Subsequently, the samples were filtered and placed in a vacuum desiccator. XRD analysis was conducted with CuKα radiation at 40 kV and 30 mA, utilizing a 2θ scan range spanning from 5° to 65°. A TA Instrument Q600 (PH407, Korea Basic Science Institute Pusan Center) was used for the TG analysis, performed between 30 and 800 °C in an N_2 atmosphere. For the MIP

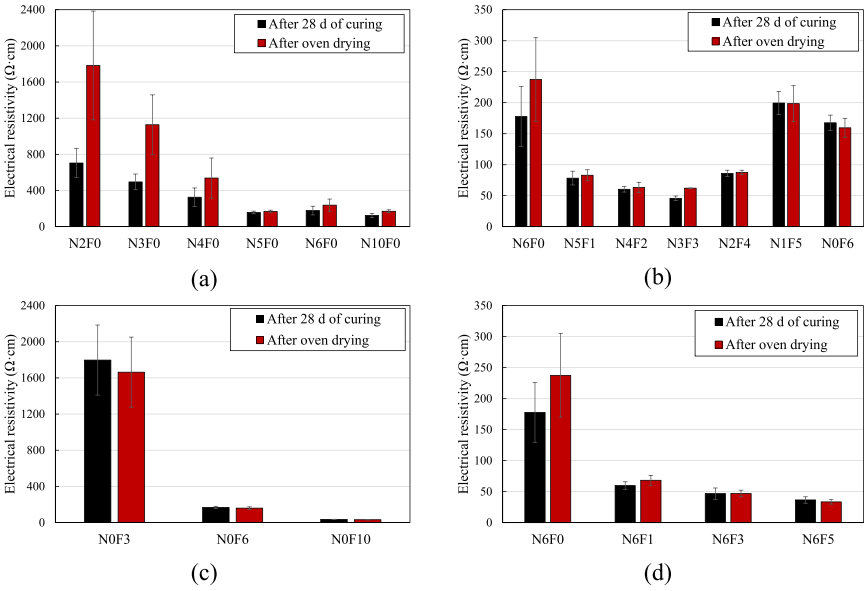

Fig. 1. Electrical resistivity of the samples after 28 days of curing and subsequent oven drying: (a) Group A, (b) Group B, (c) Group C, and (d) Group D.

analysis, the fractures were treated with isopropanol to arrest hydration then placed in a vacuum desiccator. The MIP analysis was performed utilizing an Autopore IV 9500 porosimeter (KBSI Jeonju Center), applying a maximum pressure of 414 MPa.

3. Results and discussion

3.1. Electrical and heating properties of the composites

The electrical resistivity of the samples after 28 days of curing and subsequent oven drying are shown in Fig. 1. Notably, the results of the N0F0, N1F0, and N0F1 samples were excluded because of their higher electrical resistivity (>10000 Ω cm) compared to the other samples. As shown in Fig. 1(a), the electrical resistivity of the samples exhibited a decrease as the CNT content increased, whereas there were no noticeable alterations in the electrical resistivity with increasing CNT content in the samples containing >0.5 wt% of CNT. This phenomenon occurs because of well-formed electrically conductive pathways resulting from the increase in the contact points between adjacent fillers with the increase in the amount of conductive filler (Li et al., 2007; Jang et al., 2022b). This finding is similar to the results from earlier studies in which the electrical resistance did not significantly decrease for a conductive filler content exceeding the percolation threshold (Li et al., 2007). In the samples containing >0.5 wt% of CNT, the electrical resistivity decreased after oven drying, whereas for samples with <0.5 wt% of CNT, an increase was observed. This phenomenon is likely due to ionic conduction facilitated by the water molecules (Wen and Chung, 2006; Xu et al., 2011). As ionic conduction caused by the electrolytic pore solution had a negligible effect on samples with well-established electrically conductive pathways (e.g., N5F0, N6F0, and N10F0), the electrical resistivity following oven drying did not exhibit significant changes. Conversely, in samples where the formation of electrically conductive pathways was insufficient (e.g., N2F0, N3F0, and N4F0), the electrical resistivity increased after oven drying because the effect of ionic conduction

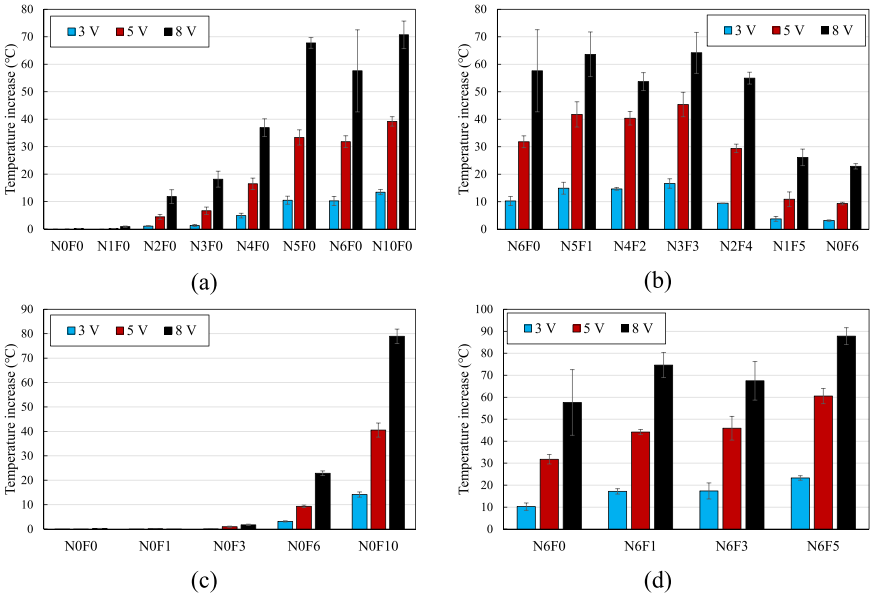

Fig. 2. Temperature increase of the samples at various input voltages: (a) Group A, (b) Group B, (c) Group C, and (d) Group D.

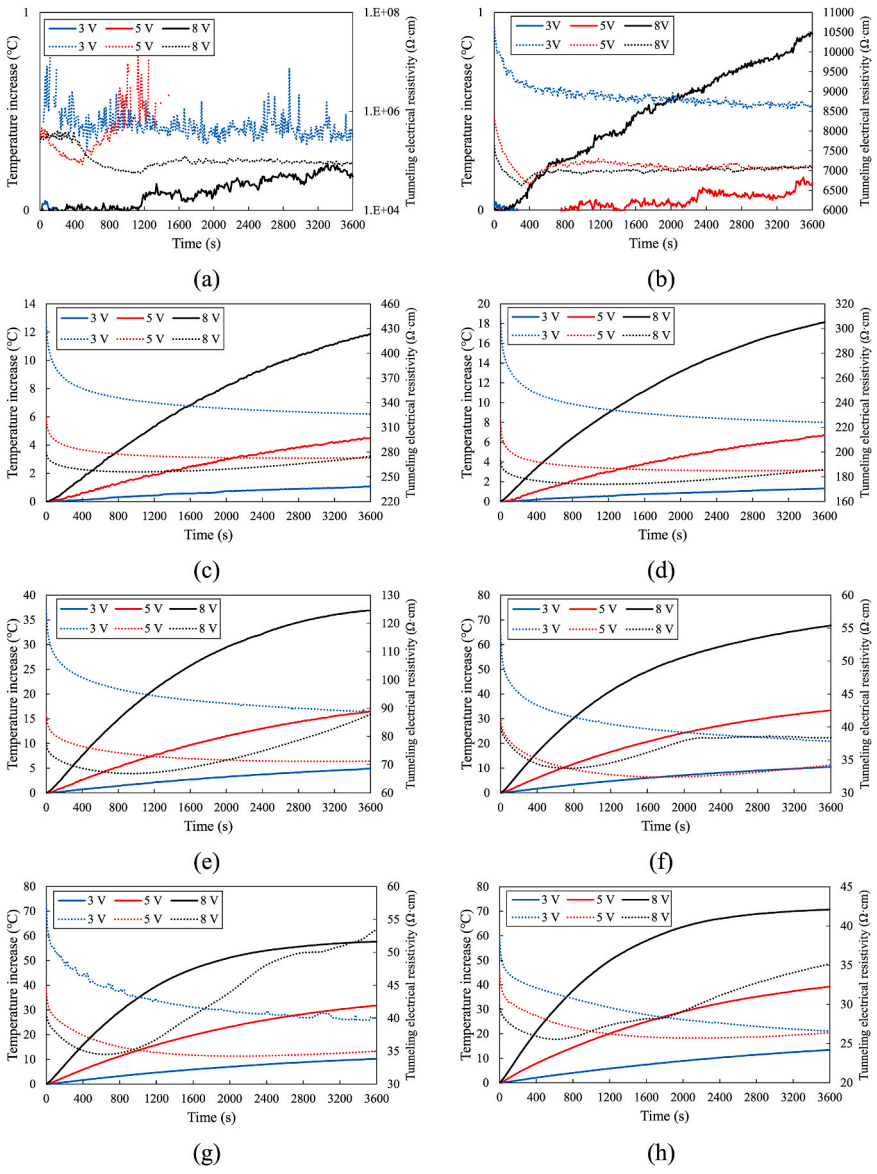

Fig. 3. Temperature increase and tunneling electrical resistivity of the samples in group A at various input voltages: (a) N0F0, (b) N1F0, (c) N2F0, (d) N3F0, (e) N4F0, (f) N5F0, (g) N6F0, and (h) N10F0.

outweighed the increase in conductivity resulting from electron transfer between conductive fillers.

As shown in Fig. 1(b)–as CF was substituted for CNT, a reduction in the electrical resistivity of the samples was observed. The N3F3 sample, which comprised 0.3 wt% of CNT and 0.3 wt% of CF, demonstrated the minimum electrical resistivity of approximately 41.3 Ω cm. This decrease in electrical resistivity of composites can be attributed to the bridging effect between CNT and CF, which has been observed in previous studies as well (Jang et al., 2023d). The electrical resistivity of the samples began to rise when the CF content surpassed that of CNT. This can be attributed to the lower electrical conductivity of CF (1×10^2–1×10^3 S/m) compared to CNT (8.3×10^3–1.9×10^5 S/m) (Cesano et al., 2020). Furthermore, the synergistic effect of CNT and CF led to a decrease in electrical resistivity when a small amount of CNT was replaced with CF. However, for samples where a large amount of CNT was substituted with CF, the electrical resistivity might be influenced more significantly by the electrical conductivity of the filler rather than the synergistic effect of CNT and CF.

The electrical resistivity of the oven-dried N0F3 sample was approximately 1fig1660 Ω cm (Fig. 1(c)), which was higher than that of the oven-dried N3F0 sample (Fig. 1(a)). However, samples with >0.6 wt % of CF content showed similar electrical resistivity to that of samples with CNT. The electrical resistivity of the N3F0 sample increased (Fig. 1 (a)), while the N0F3 sample showed a decrease in electrical resistivity following oven drying. This can be attributed to the formation of electrically conductive pathways facilitated by the micro-sized CF, which are less affected by ionic conduction, which shows similar results reported in the literature by Han et al. (2015). Lastly, as seen in Fig. 1 (d), the electrical resistivity of the samples decreased as the content of the electrically conductive filler increased.

The temperature increases of the samples at various input voltages are shown in Fig. 2. The temperature of the samples exhibited an upward trend with increasing CNT content (Fig. 2(a)). This result is consistent with Joule's first law, which states that the amount of heat generated increases as the electrical resistance decreases for the same applied voltage (Athanasopoulos et al., 2012). The temperature did not increase in the sample without CNT even at an input voltage of 8 V due to its high electrical resistivity. Conversely, the sample containing 1.0 wt% of CNT demonstrated a temperature increase of approximately 70 °C.

The samples with CNT content equal to or greater than that of CF (i.

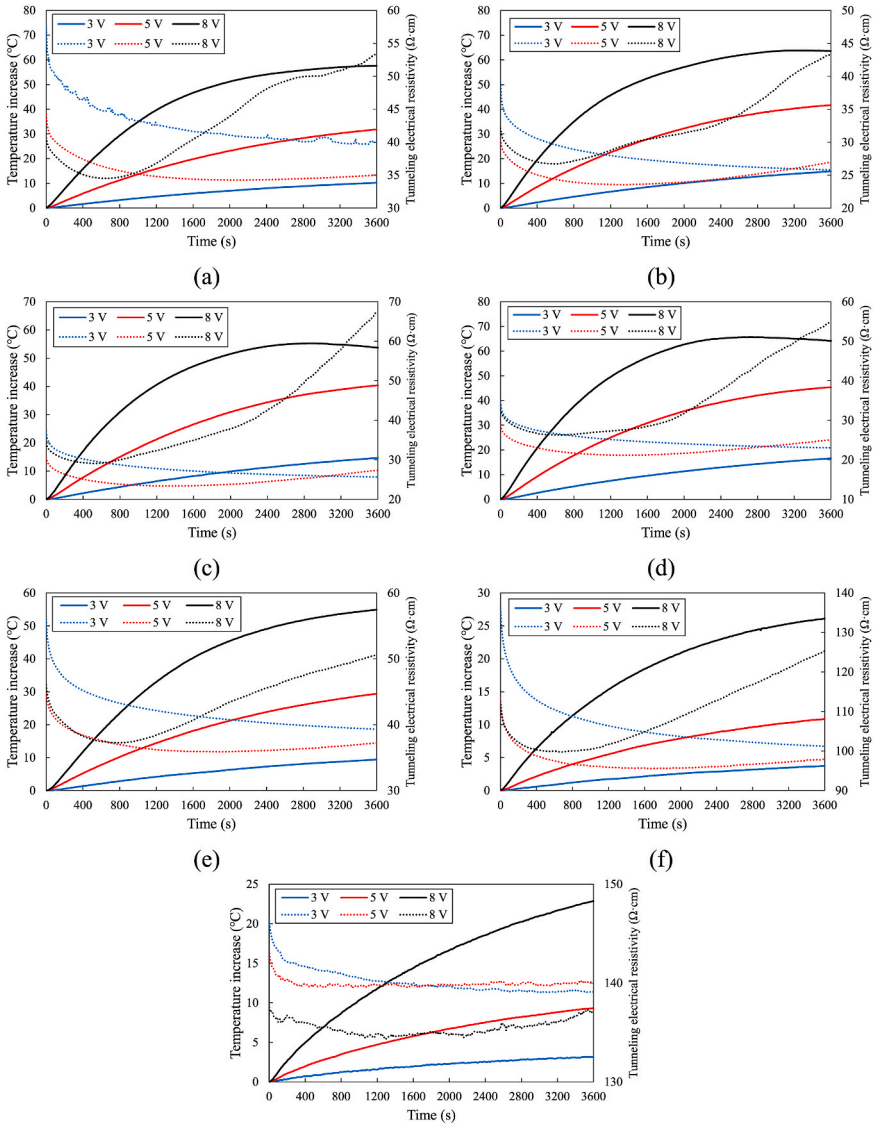

Fig. 4. Temperature increase and tunneling electrical resistivity of the samples in group B at various input voltages: (a) N6F0, (b) N5F1, (c) N4F2, (d) N3F3, (e) N2F4, (f) N1F5, and (g) N0F6.

e., N5F1, N4F2, and N3F3) showed a similar heat generation capability to the N6F0 sample, as shown in Fig. 2(b). The temperature increase at an input voltage of 8 V for the N6F0, N5F1, N4F2, and N3F3 samples were 57.6, 63.6, 53.7, and 64.1 °C, respectively. Conversely, the heat generation capacity gradually decreased with an increasing CF content relative to CNT. The temperature increase of the N0F6 sample was 22.9 °C, which was 2.5 times lower than that of the N6F0 sample. Although the electrical resistivity of N6F0 and N0F6 samples were similar (as seen in Fig. 1(b), the electrical resistivity of the N6F0 and N0F6 samples were 177.8 and 167.5 Ω cm, respectively.), the higher heat generation in the N6F0 sample compared to the N0F6 sample can be attributed to the lower thermal conductivity of CF (100–260 W/m·K) compared to that of CNT (2000–6000 W/m·K) (Hong et al., 2010)

In general, heat generation in electric heating composites predominantly occurs between the electrodes, where electrons can move directly, and then gradually transfers to the surface of the composites (Lee et al., 2020b). In addition, the thermal conductivity of CNT-incorporated composites is greater than that of CF-incorporated composites because of the high thermal conductivity of CNT (Feng et al., 2018; Zeng et al., 2014). In this study, since the temperature was measured by attaching a thermocouple to the surface of the sample, a greater temperature rise was observed in the CNT-incorporated composites with higher thermal conductivity.

As shown in Fig. 2(c), the temperature increase of the N0F10 sample at 8 V was approximately 80 °C, which was approximately four times higher than that of the N6F0 sample.

This result suggests the presence of a percolation threshold range between 0.6 wt% and 1.0 wt% in which the thermal conductivity of CF-incorporated cementitious composites rapidly increases. As shown in Fig. 2(d), the heat generation of the samples increased as a larger amount of filler was incorporated, which is consistent with Joule's first law.

3.2. NTC and PTC effects of the composites induced by electrical heating

The temperature increase and tunneling electrical resistivity of the samples in groups A, B, C, and D at various input voltages are shown in Figs. 3–6. Solid and dotted lines represent the temperature increase and tunneling electrical resistivity, respectively. As seen in Fig. 3, an NTC effect, characterized by a decrease in electrical resistivity with

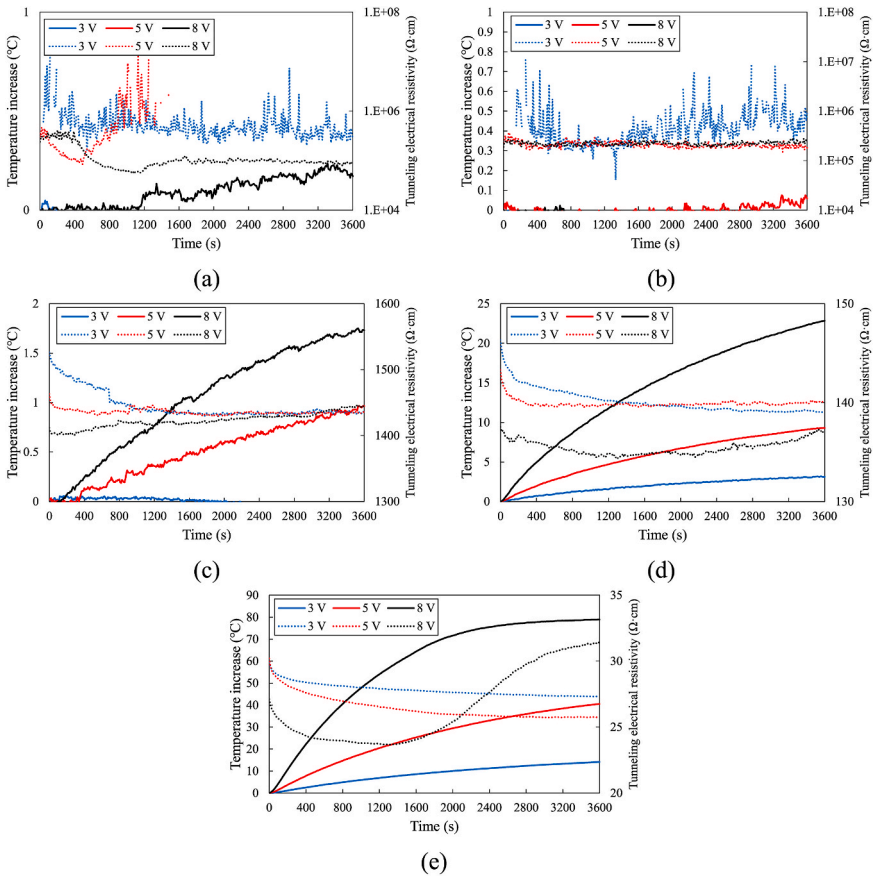

Fig. 5. Temperature increase and tunneling electrical resistivity of the samples in group C at various input voltages: (a) N0F0, (b) N0F1, (c) N0F3, (d) N0F6, and (e) N0F10.

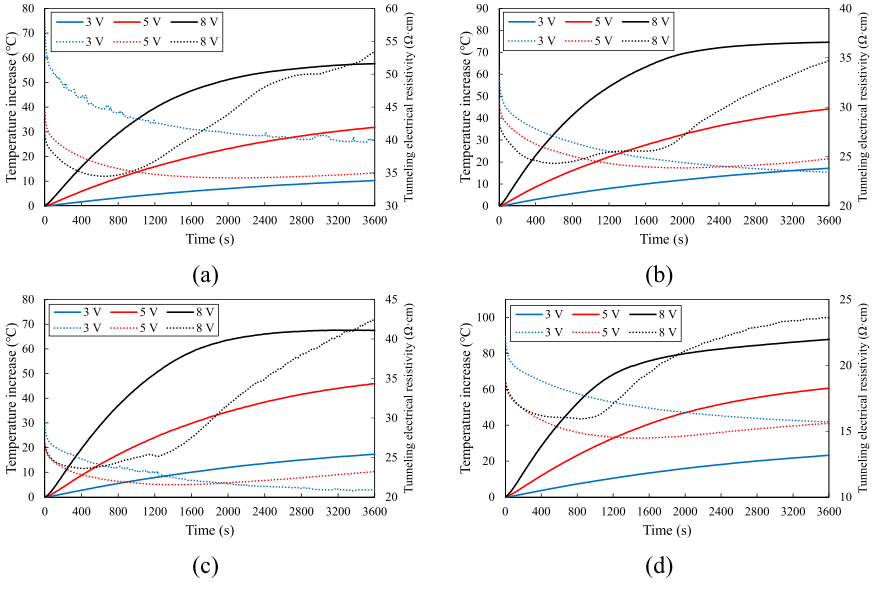

Fig. 6. Temperature increase and tunneling electrical resistivity of the samples in group D at various input voltages: (a) N6F0, (b) N6F1, (c) N6F3, and (d) N6F5.

increasing temperature, was observed in all samples regardless of the applied voltage. This phenomenon was attributed to the formation of more electrically conductive pathways by a greater number of contact points between adjacent CNT fillers produced by thermal expansion and stretching of the CNTs and thermal expansion of the cement matrix (Kim et al., 2016). For all samples, the electrical resistivity steadily decreased with increasing temperature when an input voltage of 3 V was applied. However, a PTC effect, in which the electrical resistivity increased as the temperature increased, was observed in all samples except the N0F0 and N1F0 samples at input voltages of 5 and 8 V. At 5 V, an inflection point indicating a transition from NTC to PTC effect was observed between 2000 and 3600 s, and the electrical resistivity did not show a significant

Table 2
Summary of time, temperature, and electrical resistivity at the inflection point of the samples at various input voltages.

Group	Sample ID	3 V			5 V			8 V		
		Time (s)	Temperature (°C)	Electrical resistivity (Ω·cm)	Time (s)	Temperature (°C)	Electrical resistivity (Ω·cm)	Time (s)	Temperature (°C)	Electrical resistivity (Ω·cm)
A	N0F0	-	-	-	-	-	-	-	-	-
	N1F0	-	-	-	-	-	-	-	-	-
	N2F0	-	-	-	2980	4.0	272.7	1020	4.6	255.9
	N3F0	-	-	-	2810	5.8	184.9	1180	8.9	173.9
	N4F0	-	-	-	3130	15.3	71.1	950	17.3	66.8
	N5F0	-	-	-	1780	22.4	32.4	730	28.1	33.7
	N6F0	-	-	-	2120	24.1	34.2	640	24.4	34.5
	N10F0	-	-	-	2210	30.9	25.7	610	30.2	25.5
B	N6F0	-	-	-	2120	24.1	34.2	640	24.4	34.5
	N5F1	-	-	-	1300	24.0	23.6	600	27.8	26.7
	N4F2	-	-	-	1420	24.3	23.4	540	22.5	29.1
	N3F3	-	-	-	1360	27.5	21.1	610	30.2	26.3
	N2F4	-	-	-	1900	20.5	35.9	760	22.4	37.3
	N1F5	-	-	-	1650	7.0	95.5	690	10.1	99.8
	N0F6	-	-	-	3050	8.6	139.8	1290	12.4	134.3
C	N0F0	-	-	-	-	-	-	-	-	-
	N0F1	-	-	-	-	-	-	-	-	-
	N0F3	-	-	-	-	-	-	-	-	-
	N0F6	-	-	-	3050	8.6	139.8	1290	12.4	134.3
	N0F10	-	-	-	3020	37.4	25.7	1320	57.4	23.7
D	N6F0	-	-	-	2120	24.1	34.2	640	24.4	34.5
	N6F1	-	-	-	1990	32.4	23.8	580	31.9	24.3
	N6F3	3340	16.6	20.8	1410	27.3	21.5	430	21.0	23.6
	N6F5	3580	23.2	15.7	1560	39.9	14.5	840	54.2	15.9

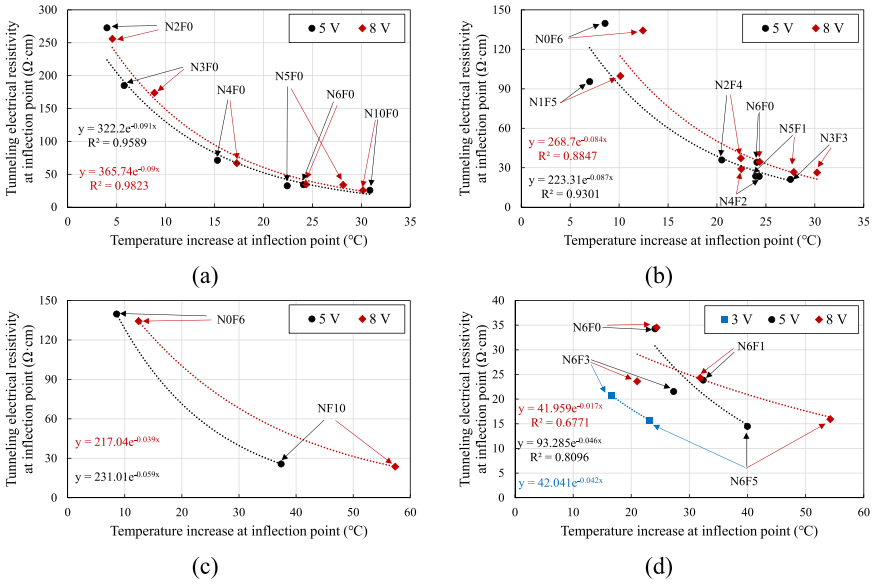

Fig. 7. Relationship between the temperature increase and tunneling electrical resistivity of the samples at inflection point: (a) Group A, (b) Group B, (c) Group C, and (d) Group D.

increase. Conversely, at 8 V, the inflection point occurred before and after approximately 1000 s, resulting in a sharp increase in electrical resistivity compared to the 5 V case. Furthermore, the electrical resistivity of the samples exhibited a more pronounced increase with higher CNT content. The occurrence of the positive temperature coefficient (PTC) effect is attributed to the impairment of electrically conductive pathways, which can be ascribed to a reduction in the contact points between the CNT fillers caused by excessive thermal expansion of the cement matrix and CNT (Zeng et al., 2014). Consequently, the inflection point was observed earlier at 8 V compared to 5 V due to the higher temperature rise. Similar trends to those observed in group A were noted for groups B, C, and D (Figs. 4–6).

Table 2 presents summary of the time, temperature, and electrical resistivity at the inflection point of the samples at various input voltages. In group A, the temperature increase and electrical resistivity at the inflection point were almost similar for each mix proportion, regardless of the input voltage. These observations are consistent with prior research, wherein the NTC effect stemmed from the initial thermal expansion of both the cement matrix and CNT during the onset of heat generation. Conversely, the PTC effect arose due to the heightened thermal expansion of the cement matrix as temperature increased (Chu and Park, 2016). Moreover, it can be inferred from these results that the specific occurrence point of the inflection point is associated with changes in the electrical resistivity of the samples due to thermal expansion. For example, when an input voltage of 3 V was applied, the electrical resistivity of the N2F0, N3F0, N4F0, N5F0, N6F0, and N10F0

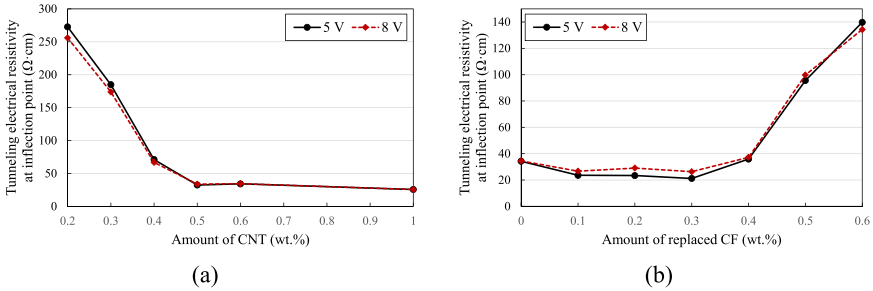

Fig. 8. Relationship between the amount of conductive filler and electrical resistivity at the inflection point of the samples: (a) Group A and (b) Group B.

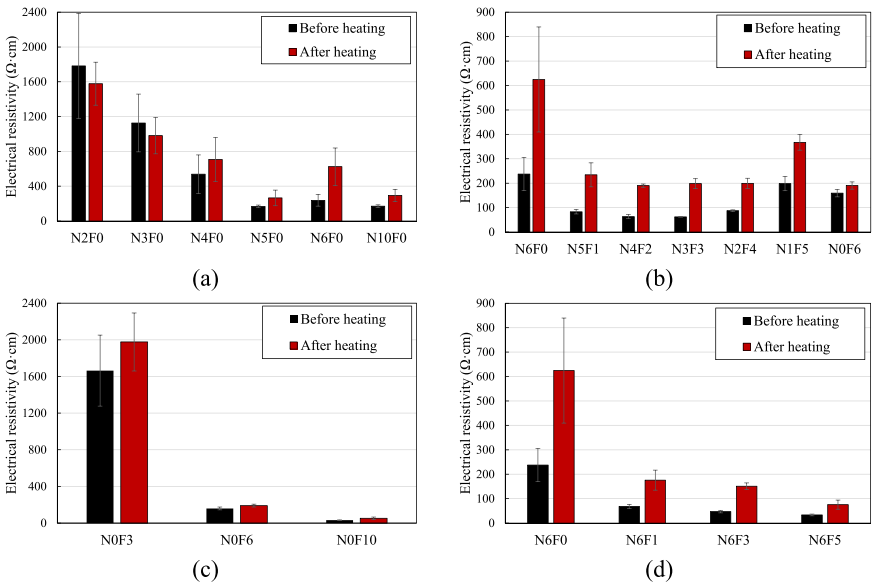

Fig. 9. Electrical resistivity of the samples before and after the heating test: (a) Group A, (b) Group B, (c) Group C, and (d) Group D.

samples at 3600 s were measured at 326.1, 224.0, 88.7, 37.8, 39.7, and 26.6 Ω cm, respectively. However, these values were lower than the electrical resistivity at which the inflection point occurred for input voltages of 5 V and 8 V. In particular, the occurrence of the PTC effect is influenced by the content of conductive fillers, as observed in the N1F0 sample, where a PTC effect was observed despite a modest temperature increase of approximately 4–5 °C. Similar results to group A were observed in groups B, C, and D.

Fig. 7 shows the relationship between the temperature increase and tunneling electrical resistivity of the samples at the inflection point for each group. The presence of a consistent relationship between electrical resistivity and temperature increase at the inflection point, regardless of the applied voltage, was confirmed. In particular, the electrical resistivity at the inflection point remained similar for the same mix proportion regardless of the temperature increase caused by the input voltage. This suggests that the occurrence point of the inflection point is associated with a specific electrical resistivity value of the sample, which is influenced by the thermal expansion resulting from an increase in temperature. In the case of group D, no clear trend in the occurrence of the inflection point was observed due to the accelerated heat generation in samples with increasing applied voltage. This can be attributed to their low electrical resistivity resulting from a high content of conductive filler. Nonetheless, the electrical resistivity at the inflection point remained relatively constant across the samples.

The relationship between the amount of conductive filler and the electrical resistivity at the inflection point of the sample in groups A and B is shown in Fig. 8. As shown in Fig. 8 (a), it can be observed that the tunneling electrical resistivity at the inflection point gradually decreased with an increase in the CNT content, while it did not exhibit a significant reduction for CNT contents exceeding 0.5 wt%. Several studies have investigated the existence of a percolation threshold at which the electrical resistivity of the composite incorporating the conductive filler drastically decreases. This result indicates that the tunneling electrical resistivity at the inflection point also exhibits a similar trend as the percolation threshold associated with the electrical resistivity of the samples. In addition, the tunneling electrical resistivity of the group B samples at the inflection point increased as the CNT was replaced by CF.

The electrical resistivity of the samples before and after the heating test are shown in Fig. 9. The results of N0F0, N1F0, and N0F1 samples were excluded due to the high electrical resistivity compared to other samples. After the monotonic heating test, the electrical resistivity of the majority of samples exhibited a significant increase compared to the non-heating sample, with the exception of the N2F0 and N3F0 samples. The observed increase in electrical resistivity is considered the damage inflicted upon the cement matrix and conductive pathways due to the rapid temperature rise during the monotonic heating test. However, the electrical resistivity of the N2F0 and N3F0 samples was found to be lower after the heating test. This can be attributed to the fact that the temperature increase during the heating test was insufficient to cause damage to the cement matrix and conductive pathways, likely due to the low CNT content in the N2F0 and N3F0 samples.

3.3. *Microstructure change of the composites induced by electrical heating*

The XRD patterns of selected samples before and after the heating

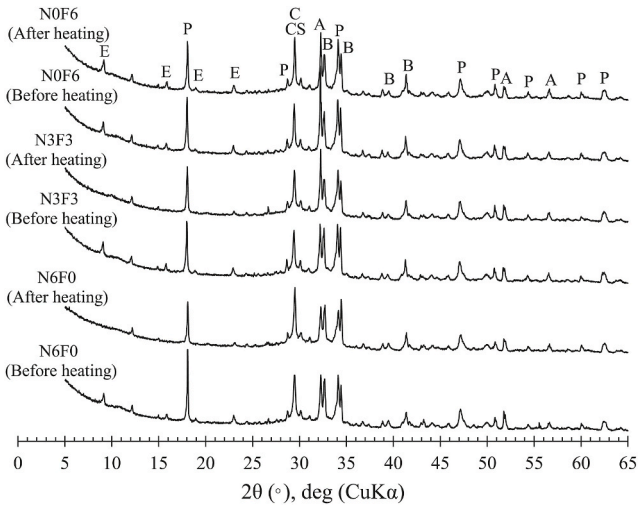

Fig. 10. XRD patterns of selected samples before and after the heating test. The annotations indicate the following: E: ettringite, P: portlandite, C: calcite, CS: C–S–H, A: alite, and B: belite.

test are shown in Fig. 10. The XRD patterns show that the main reaction products are ettringite ($Ca_6Al_2(SO_4)_3(OH)_{12} \bullet 26H_2O$), portlandite ($Ca(OH)_2$), calcite ($CaCO_3$), and calcium silicate hydrate (C–S–H). Peaks corresponding to the unreacted cement phases, alite (Ca_3SiO_5), and belite (β-Ca_2SiO_4), were also observed. There were no significant differences in the XRD patterns according to the CNT and CF contents. Notably, the peaks associated with ettringite were present in the N6F0 and N3F3 samples before the heating test but became undetectable after the heating test. In contrast, the peaks related to ettringite were observed persistently in the N0F6 sample even after the heating test.

The thermograms and derivative thermograms (DTG) of selected samples before and after the heating test are shown in Fig. 11. The major observable mass loss humps in the DTG curves of the samples denote the dehydration of the ettringite and C–S–H at approximately 100 °C, the dehydration of portlandite at around 420 °C, and the decarbonation of carbonated phases and the presence of unhydrated cement at 600–700 °C (Seo et al., 2018; Park et al., 2019). The peaks in ettringite and C–S–H at approximately 100 °C for the N6F0 and N3F3 samples were observed to decrease significantly after the heating test. Conversely, there were no substantial changes observed in the TG/DTG graph of the N0F6 sample before and after the heating test.

Based on the XRD and TG/DTG findings, it can be inferred that the temperature increase of the N6F0 and N3F3 samples during the monotonic heating test led to changes in the reaction product associated with the chemical structure, primarily owing to the dehydration of ettringite and evaporation of the pore solution. This phenomenon promotes the PTC effect in the samples. In fact, most of the samples exhibited a distinct and rapid PTC effect when 8 V was applied. Although the surface temperature of the samples increased by approximately 60 °C (refer to Fig. 2), it is important to note that the temperature at the center of the sample is expected to be higher than that at the surface (Jang et al., 2020, 2021c, 2023e). Consequently, the temperature at the center of the sample is anticipated to reach the necessary level for the dehydration of ettringite. Conversely, in the case of the N0F6 sample, ettringite was observed both before and after the heating test, likely indicating that the temperature required for dehydration of ettringite was not attained during the heating test. For this reason, a relatively weak PTC effect was observed in the N0F6 sample.

Fig. 12 shows the cumulative pore volume and first derivatives of the cumulative curves of the selected samples before and after the heating

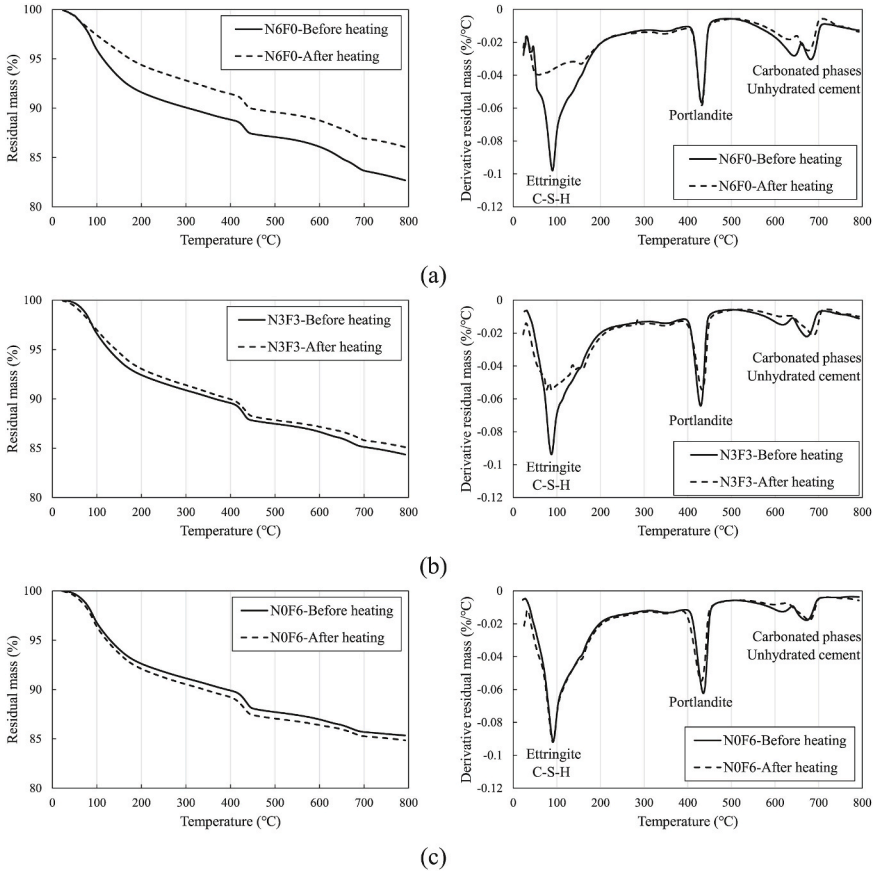

Fig. 11. Thermograms and derivative thermograms of selected samples before and after the heating test: (a) N6F0, (b) N3F3, and (c) N0F6.

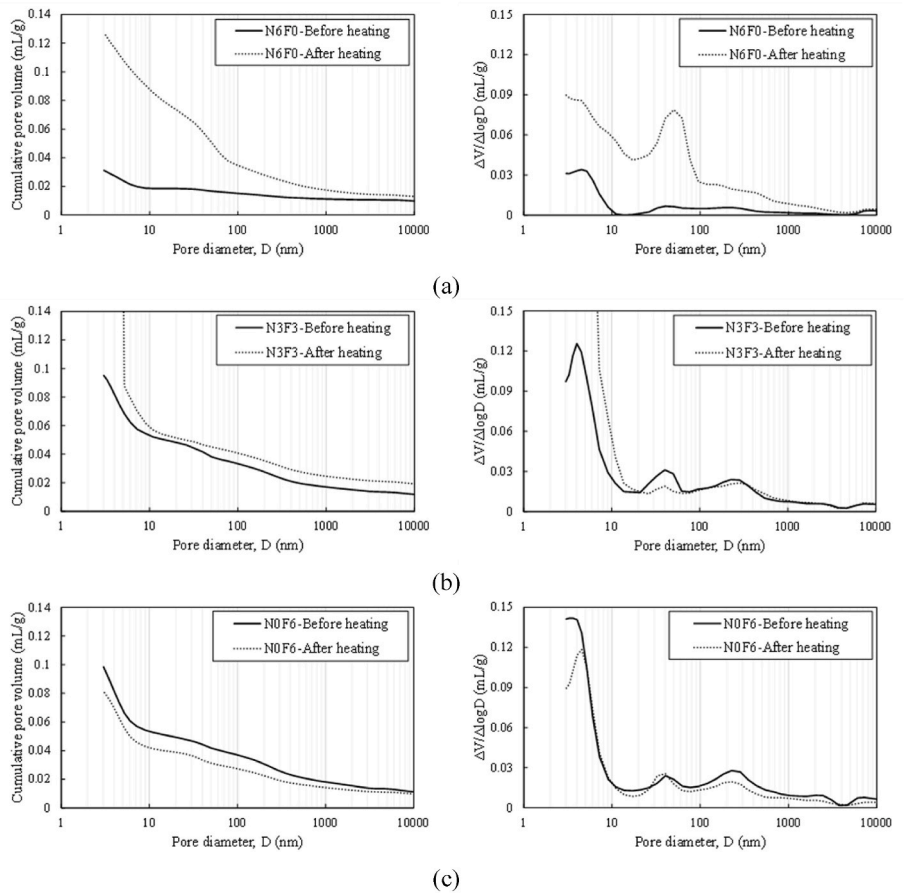

Fig. 12. Cumulative pore volume and first derivatives of the cumulative curves of the selected samples before and after the heating test: (a) N6F0, (b) N3F3, and (c) N0F6.

test. The result for the N3F3 sample after heating test is not available due to a fracture of this sample during the MIP process. The cumulative pore volume of the N6F0 sample significantly increased after heating test. The pore structure of the N6F0 sample before the heating test consisted of pores with diameters <10 nm; however, after the heating test, there was a drastic increase in pores with diameters between 10 nm and 1000 nm. Conversely, the porosity of the N0F6 sample decreased after the heating test. As a reslut, the electrical resistivity of the samples significantly increased due to the change in the physicochemical structure of the cement matrix after the heating test.

Consequently, the electrical resistivity of the samples greatly increased owing to the change in the physicochemical components and structure of the cement matrix during the heating test. The decomposition of the hydration product and the creation of additional pores occurred as the temperature increased, which accelerated the PTC effect more rapidly.

4. Conclusions

The present study investigated the influence of conductive filler content on NTC/PTC effects and microstructural changes of cementitious composites incorporating CNT and CF under electric heating conditions. The relationship between the temperature increase and the change in the electrical resistivity of the samples was analyzed through the monotonic heating test. In addition, microstructural changes of the composites were observed via XRD, TG, and MIP analyses. The key outcomes of this investigation can be outlined as follows:

(1) The electrical resistivity of the samples decreased with an increase in the conductive filler content. When CNT was replaced with CF, the electrical resistivity decreased owing to the synergistic effect of CNT and CF, while it increased with higher CF content. This can be attributed to the lower electrical conductivity of CF compared to that of CNT.
(2) The heat generation of the samples increased with lower electrical resistivity, in accordance with Joule's first law. As CF replaced CNT in the samples, the amount of heat generated decreased, owing to the low thermal conductivity of CF.
(3) The NTC and PTC effects were observed in most of the samples, and the temperature at the inflection point increased with an increase in the content of the conductive filler. The electrical resistivity at the inflection point in the same mix proportion is almost similar regardless of temperature rise according to the input voltage.
(4) Changes in the physicochemical structure of the samples were observed during electric heating. Increasing the temperature of the sample led to the decomposition of the hydration product and the creation of additional more pores, thereby accelerating the PTC effect.

CRediT authorship contribution statement

H.N. Yoon: Writing – original draft, Formal analysis, Data curation, Conceptualization. **Jinho Bang:** Validation, Visualization. **Daeik Jang:** Validation, Methodology, Investigation. **Beomjoo Yang:** Writing – review & editing, Writing – original draft, Resources, Conceptualization.

Declaration of competing interest

"Investigation on NTC/PTC effects of cement-based self-heating

composites with varied conductive filler contents" by Yoon et al.

We wish to confirm that there are no known conflicts of interest associated with this publication and there has been no significant financial support for this work that could have influenced its outcome.

We confirm that the manuscript has been read and approved by all named authors and that there are no other persons who satisfied the criteria for authorship but are not listed. We further confirm that the order of authors listed in the manuscript has been approved by all of us.

We confirm that we have given due consideration to the protection of intellectual property associated with this work and that there are no impediments to publication, including the timing of publication, with respect to intellectual property. In so doing we confirm that we have followed the regulations of our institutions concerning intellectual property.

We understand that the Corresponding Author is the sole contact for the Editorial process. He/she is responsible for communicating with the other authors about progress, submissions of revisions and final approval of proofs. We confirm that we have provided a current, correct email address which is accessible by the corresponding author byang@cbnu.ac.kr (BY).

Data availability

No data was used for the research described in the article.

Acknowledgments

This study was supported by the National Research Foundation of Korea (NRF) grant funded by the Korea government (MSIT) (2020R1C1C1005063 and 2022R1A4A3029737).

References

Athanasopoulos, N., Sikoutris, D., Panidis, T., Kostopoulos, V., 2012. Numerical investigation and experimental verification of the Joule heating effect of polyacrylonitrile-based carbon fiber tows under high vacuum conditions. J. Compos. Mater. 46, 2153–2165. https://doi.org/10.1177/0021998311430159.

Azhari, F., Banthia, N., 2012. Cement-based sensors with carbon fibers and carbon nanotubes for piezoresistive sensing. Cem. Concr. Compos. 34, 866–873. https://doi.org/10.1016/j.cemconcomp.2012.04.007.

Cesano, F., Uddin, M.J., Lozano, K., Zanetti, M., Scarano, D., 2020. All-carbon conductors for electronic and electrical wiring applications. Front Mater 7. https://doi.org/10.3389/fmats.2020.00219.

Chien, A.T., Cho, S., Joshi, Y., Kumar, S., 2014. Electrical conductivity and Joule heating of polyacrylonitrile/carbon nanotube composite fibers. Polymer 55, 6896–6905. https://doi.org/10.1016/j.polymer.2014.10.064.

Chu, K., Park, S.H., 2016. Electrical heating behavior of flexible carbon nanotube composites with different aspect ratios. J. Ind. Eng. Chem. 35, 195–198. https://doi.org/10.1016/j.jiec.2015.12.033.

Ding, S., Xiang, Y., Ni, Y.Q., Thakur, V.K., Wang, X., Han, B., Ou, J., 2022. In-situ synthesizing carbon nanotubes on cement to develop self-sensing cementitious composites for smart high-speed rail infrastructures. Nano Today 43, 101438. https://doi.org/10.1016/j.nantod.2022.101438.

Ding, S., Wang, X., Qiu, L., Ni, Y.Q., Dong, X., Cui, Y., Ashour, A., Han, B., Ou, J., 2023. Self-sensing cementitious composites with hierarchical carbon fiber-carbon nanotube composite fillers for crack development monitoring of a maglev girder. Small 19, 2206258. https://doi.org/10.1002/smll.202206258.

Feng, A., Jia, Z., Yu, Q., Zhang, H., Wu, G., 2018. Preparation and characterization of carbon nanotubes/carbon fiber/phenolic composites on mechanical and thermal conductivity properties. Nano 13, 1850037. https://doi.org/10.1142/S1793292018500376.

Han, B., Zhang, L., Sun, S., Yu, X., Dong, X., Wu, T., Ou, J., 2015. Electrostatic self-assembled carbon nanotube/nano carbon black composite fillers reinforced cement-based materials with multifunctionality. Composer Part A Appl Sci Manuf 79, 103–115. https://doi.org/10.1016/j.compositesa.2015.09.016.

Hong, J., Park, D.W., Shim, S.E., 2010. A review on thermal conductivity of polymer composites using carbon-based fillers: carbon nanotubes and carbon fibers. Carbon Lett 11, 347–356. https://doi.org/10.5714/CL.2010.11.4.347.

Jang, J.-U., Cha, J.E., Lee, S.H., Kim, J., Yang, B., Kim, S.Y., Kim, S.H., 2020. Enhanced electrical and electromagnetic interference shielding properties of uniformly dispersed carbon nanotubes filled composite films via solvent-free process using ring-opening polymerization of cyclic butylene terephthalate. Polymer 186, 122030. https://doi.org/10.1016/j.polymer.2019.122030.

Jang, D., Yoon, H.N., Seo, J., Park, S., Kil, T., Lee, H.K., 2021a. Improved electric heating characteristics of CNT-embedded polymeric composites with an addition of silica aerogel. Compos. Sci. Technol. 212, 108866 https://doi.org/10.1016/j.compscitech.2021.108866.

Jang, D., Yoon, H.N., Farooq, S.Z., Lee, H.K., Nam, I.W., 2021b. Influence of water ingress on the electrical properties and electromechanical sensing capabilities of CNT/cement composites. J. Build. Eng. 42, 103065 https://doi.org/10.1016/j.jobe.2021.103065.

Jang, D., Yoon, H.N., Seo, J., Lee, H.K., Kim, G.M., 2021c. Effects of silica aerogel inclusion on the stability of heat generation and heat-dependent electrical characteristics of cementitious composites with CNT. Cem. Concr. Compos. 115, 103861 https://doi.org/10.1016/j.cemconcomp.2020.103861.

Jang, D., Yoon, H.N., Seo, J., Park, S., 2022a. Enhanced electrical heating capability of CNT-embedded cementitious composites exposed to water ingress with addition of silica aerogel. Ceram. Int. 13356–13365. https://doi.org/10.1016/j.ceramint.2022.01.216.

Jang, D., Yoon, H.N., Seo, J., Yang, B., 2022b. Effects of exposure temperature on the piezoresistive sensing performances of MWCNT-embedded cementitious sensor. J. Build. Eng. 47, 103816 https://doi.org/10.1016/j.jobe.2021.103816.

Jang, D., Yoon, H.N., Seo, J., Yang, B., Jang, J.G., Park, S., 2023a. Effect of carbonation curing regime on electric heating performance of CNT/cement composites. J. Build. Eng. 73, 106815 https://doi.org/10.1016/j.jobe.2023.106815.

Jang, D., Bang, J., Jeon, H., 2023b. Impact of silica aerogel addition on the electrical and piezo-resistive sensing stability of CNT-embedded cement-based sensors exposed to varied environments. J. Build. Eng. 78, 107700 https://doi.org/10.1016/j.jobe.2023.107700.

Jang, D., Bang, J., Yoon, H.N., Kim, Y.-K., Lee, J.H., Yoon, H., Cheon, S.-H., Yang, B., 2023c. Directionally sensitive cement-based sensor using carbon nanotube and carbonyl iron powder (CNT@CIP)-based nanohybrid clusters. Construct. Build. Mater. 409, 134116 https://doi.org/10.1016/j.conbuildmat.2023.134116.

Jang, D., Yoon, H.N., Yang, B., Khalid, H.R., 2023d. Cyclic heat-generation and storage capabilities of self-heating cementitious composite with an addition of phase change material. Construct. Build. Mater. 369, 130512 https://doi.org/10.1016/j.conbuildmat.2023.130512.

Jang, D., Yoon, H.N., Park, S., Kim, S., Bae, J.H., Kim, N., Kim, G.M., Seo, J., 2023e. Pressure-aided fabrication of CNT-incorporated composites made with fly ash or slag-blended Portland cement. Compos. Struct. 313, 116926 https://doi.org/10.1016/j.compstruct.2023.116926.

Jang, D., Jang, W., Bang, J., Kim, M., Yang, B., 2024. Absorption-dominant electromagnetic interference (EMI) shielding cement with hollow glass microsphere (HGM) at elevated temperatures. https://doi.org/10.21203/rs.3.rs-3990304/v1.

Jeong, Y.G., Jeon, G.W., 2013. Microstructure and performance of multiwalled carbon nanotube/m-aramid composite films as electric heating elements. ACS Appl. Mater. Interfaces 5, 6527–6534. https://doi.org/10.1021/am400892k.

Kil, T., Jang, D.I., Yoon, H.N., Yang, B., 2022. Machine learning-based predictions on the self-heating characteristics of nanocomposites with hybrid fillers. Comput. Mater. Continua (CMC) 71, 4487–4502. https://doi.org/10.32604/cmc.2022.020940.

Kim, G.M., Naeem, F., Kim, H.K., Lee, H.K., 2016. Heating and heat-dependent mechanical characteristics of CNT-embedded cementitious composites. Compos. Struct. 136, 162–170. https://doi.org/10.1016/j.compstruct.2015.10.010.

Kim, G.M., Park, S.M., Ryu, G.U., Lee, H.K., 2017. Electrical characteristics of hierarchical conductive pathways in cementitious composites incorporating CNT and carbon fiber. Cem. Concr. Compos. 82, 165–175. https://doi.org/10.1016/j.cemconcomp.2017.06.004.

Kim, G.M., Yang, B.J., Yoon, H.N., Lee, H.K., 2018. Synergistic effects of carbon nanotube and carbon fiber on heat generation and electrical characteristics of cementitious composites. Carbon 134, 283–292. https://doi.org/10.1016/j.carbon.2018.03.070.

Lee, H., Yu, W., Loh, K.J., Chung, W., 2020a. Self-heating and electrical performance of carbon nanotube-enhanced cement composites. Construct. Build. Mater. 250, 118838 https://doi.org/10.1016/j.conbuildmat.2020.118838.

Lee, H., Park, S., Park, S., Chung, W., 2020b. Enhanced detection systems of filling rates using carbon nanotube cement grout. Nanomaterials 10, 10. https://doi.org/10.3390/nano10010010.

Li, J., Ma, P.C., Chow, W.S., To, C.K., Tang, B.Z., Kim, J.K., 2007. Correlations between percolation threshold, dispersion state, and aspect ratio of carbon nanotubes. Adv. Funct. Mater. 17, 3207–3215. https://doi.org/10.1002/adfm.200700065.

Liu, Y., Wang, M., Tian, W., Qi, B., Lei, Z., Wang, W., 2019. Ohmic heating curing of carbon fiber/carbon nanofiber synergistically strengthening cement-based composites as repair/reinforcement materials used in ultra-low temperature environment. Composer Part A Appl Sci Manuf 125, 105570. https://doi.org/10.1016/j.compositesa.2019.105570.

Meng, X., Liu, Y., Huang, M., Cao, J.P., 2017. Flexible perfluoroalkoxy films filled with carbon nanotubes and their electric heating property. J. Appl. Polym. Sci. 134 https://doi.org/10.1002/app.44782.

Neitzert, H.C., Vertuccio, L., Sorrentino, A., 2011. Epoxy/MWCNT composite as temperature sensor and Electrical heating element. IEEE Trans. Nanotechnol. 10, 688–693. https://doi.org/10.1109/TNANO.2010.2068307.

Park, H.M., Park, S.M., Lee, S.-M., Shon, I.-J., Jeon, H., Yang, B.J., 2019. Automated generation of carbon nanotube morphology in cement composite via data-driven approaches. Composites, Part B 167, 51–62. https://doi.org/10.1016/j.compositesb.2018.12.011.

Seo, J.H., Park, S.M., Lee, H.K., 2018. Evolution of the binder gel in carbonation-cured Portland cement in an acidic medium. Cement Concr. Res. 109, 81–89. https://doi.org/10.1016/j.cemconres.2018.03.014.

Shin, Y.C., Novin, E., Kim, H., 2015. Electrical and thermal conductivities of carbon fiber composites with high concentrations of carbon nanotubes. Int. J. Precis. Eng. Manuf. 16, 465–470. https://doi.org/10.1007/s12541-015-0063-8.

Wen, S., Chung, D.D.L., 2006. The role of electronic and ionic conduction in the electrical conductivity of carbon fiber reinforced cement. Carbon 44, 2130–2138. https://doi.org/10.1016/j.carbon.2006.03.013.

Xiang, Z.D., Chen, T., Li, Z.M., Bian, X.C., 2009. Negative temperature coefficient of resistivity in lightweight conductive carbon nanotube/polymer composites. Macromol. Mater. Eng. 294, 91–95. https://doi.org/10.1002/mame.200800273.

Xu, J., Yao, W., Wang, R., 2011. Nonlinear conduction in carbon fiber reinforced cement mortar. Cem. Concr. Compos. 33, 444–448. https://doi.org/10.1016/j.cemconcomp.2010.10.007.

Yoon, H.N., Jang, D., Lee, H.K., Nam, I.W., 2021. Influence of carbon fiber additions on the electromagnetic wave shielding characteristics of CNT-cement composites. Construct. Build. Mater. 269, 121238 https://doi.org/10.1016/j.conbuildmat.2020.121238.

Yoon, H.N., Jang, D., Kil, T., Lee, H.K., 2023. Influence of various deterioration factors on the electrical properties of conductive cement paste. Construct. Build. Mater. 367, 130289 https://doi.org/10.1016/j.conbuildmat.2022.130289.

Zeng, Y., Lu, G., Wang, H., Du, J., Ying, Z., Liu, C., 2014. Positive temperature coefficient thermistors based on carbon nanotube/polymer composites. Sci. Rep. 4, 6684. https://doi.org/10.1038/srep06684.

Zhou, H.W., Mishnaevsky, L., Yi, H.Y., Liu, Y.Q., Hu, X., Warrier, A., Dai, G.M., 2016. Carbon fiber/carbon nanotube reinforced hierarchical composites: effect of CNT distribution on shearing strength. Compos. B Eng. 88, 201–211. https://doi.org/10.1016/j.compositesb.2015.10.035.